International Journal of Nanomedicine

Dovepress
open access to scientific and medical research

Open Access Full Text Article

ORIGINAL RESEARCH

A Multi-Component Nano-Co-Delivery System Utilizing Astragalus Polysaccharides as Carriers for Improving Biopharmaceutical Properties of Astragalus Flavonoids

Bing Yang[1,*], Xiaochun Wu[1,*], Jingqi Zeng[1], Jinjing Song[1], Tianhao Qi[1], Yanjun Yang[1], Dingkun Liu[1], Yulin Mo[1], Miao He[2], Liang Feng[1], Xiaobin Jia[1]

[1]School of Traditional Chinese Pharmacy, State Key Laboratory of Natural Medicines, China Pharmaceutical University, Nanjing, 211198, People's Republic of China; [2]College of Pharmacy, Dali University, Dali, Yunnan, People's Republic of China

*These authors contributed equally to this work

Correspondence: Xiaobin Jia; Liang Feng, School of Traditional Chinese Pharmacy, China Pharmaceutical University, Nanjing, 211198, People's Republic of China, Email jiaxiaobin2015@163.com; wenmoxiushi@163.com

Purpose: Enhancing the dissolution, permeation and absorption of active components with low solubility and poor permeability is crucial for maximizing therapeutic efficacy and optimizing functionality. The objective of this study is to investigate the potential of natural polysaccharides as carriers to improve the biopharmaceutical properties of active components.

Methods: In this study, we employed four representative flavonoids in Astragali Radix, namely Calycosin-*7-O-β-D*-glucoside (CAG), Ononin (ON), Calycosin (CA) and Formononetin (FMN), as a demonstration to evaluate the potential of Astragalus polysaccharides (APS) as carriers to improve the biopharmaceutical properties, sush as solubility, permeability, and absorption in vivo. In addition, the microstructure of the flavonoids-APS complexes was characterized, and the interaction mechanism between APS and flavonoids was investigated using multispectral technique and molecular dynamics simulation.

Results: The results showed that APS can self-assemble into aggregates with a porous structure and large surface area in aqueous solutions. These aggregates can be loaded with flavonoids through weak intermolecular interactions, such as hydrogen bonding, thereby improving their gastrointestinal stability, solubility, permeability and absorption in vivo.

Conclusion: We discovered the self-assembly properties of APS and its potential as carriers. Compared with introducing external excipients, the utilization of natural polysaccharides in plants as carriers may have a unique advantage in enhancing dissolution, permeation and absorption.

Keywords: astragalus polysaccharides, flavonoids, self-assembly, solubility, permeability, natural carrier

Introduction

Multi-component nano-co-delivery system has been recognized as a highly effective strategy for improving the biopharmaceutical properties of low solubility and poor permeability components.[1–3] Recent research has demonstrated that multiple components can form co-delivery system through various interactions, including hydrogen bonding, π-π stacking, electrostatic interactions and Van der Waals forces.[4,5] Natural polysaccharides, derived from natural sources, are polymeric carbohydrates that possess distinctive chemical properties.[6–8] They demonstrate outstanding characteristics such as water solubility, dispersion stability, biocompatibility, and biodegradability. Therefore, natural polysaccharides hold immense promise as carriers.

In recent years, an increasing body of literature suggests that natural polysaccharides may exhibit interactions with small molecule active components,[9–11] thereby potentially contributing to their therapeutic potential in the treatment of

Received: 11 August 2023
Accepted: 18 October 2023
Published: 14 November 2023

Graphical Abstract

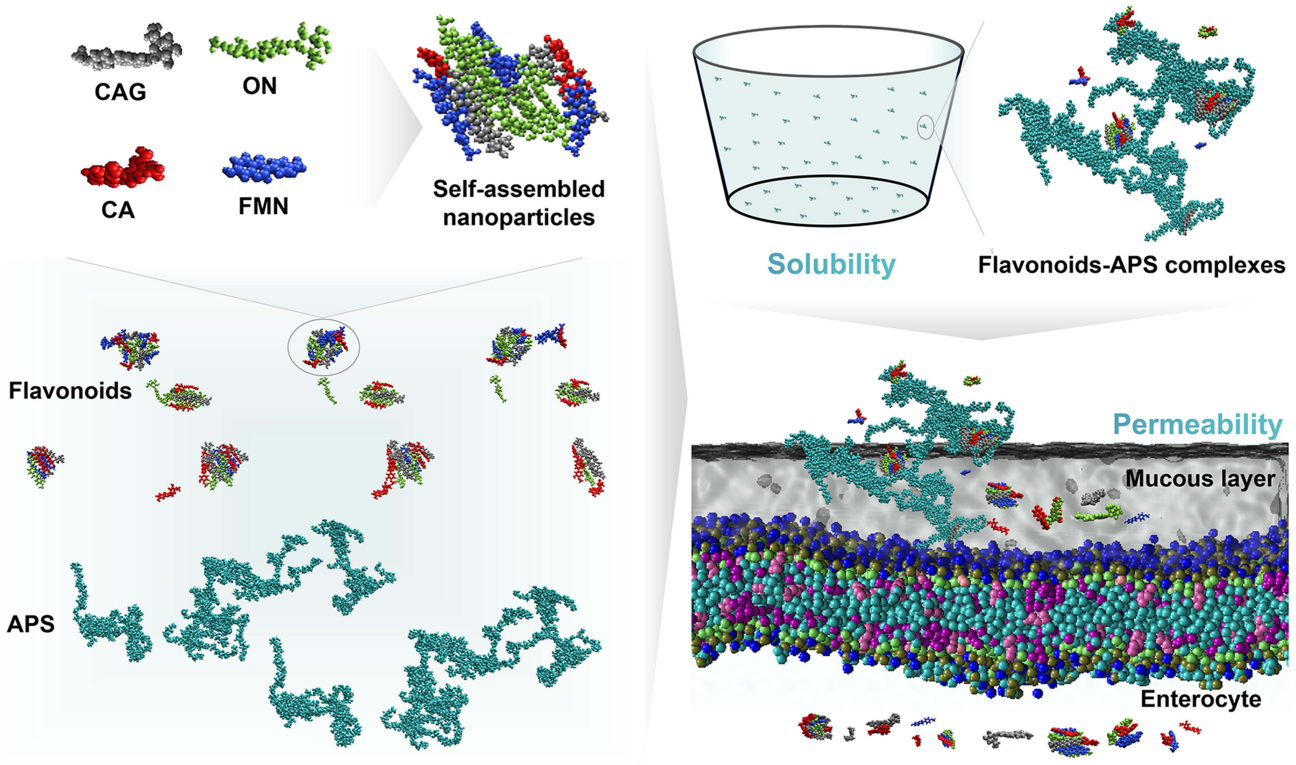

various diseases. For instance, it has been reported that glycyrrhiza polysaccharides can enhance the efficacy of active components present in aconite,[12] while cistanche polysaccharides may enhance the absorption of pineal glycosides.[13] Consequently, natural polysaccharides may play a crucial role in improving the hydrophily and bioavailability of insoluble components.[14] However, the interaction between natural polysaccharides and insoluble components and their synergistic mechanisms, have yet to be fully elucidated and require further exploration.

Astragali Radix is a commonly used plant with a homology of food and medicine, belonging to Astragalus genus in Leguminosae family. Flavonoids are a type of active component in Astragali Radix that exhibit various beneficial effects, such as anti-inflammatory, immune regulation, anti-tumor, and cardiovascular protective effects.[15,16] However, these flavonoids suffer from limitations, such as low solubility, poor permeability, low gastrointestinal absorption and low bioavailability.[17] Therefore, improving the bioavailability of flavonoids is a challenging issue. In our previous study, we made an interesting discovery that the in vivo blood concentration of flavonoids can be significantly increased when co-administered with Astragalus polysaccharides (APS). Additionally, we also observed the co-loading characteristics of flavonoids and APS in their co-solvent system. Based on these findings, we have proposed a hypothesis that APS can serve as a natural carrier, forming nanoparticles for the encapsulation of small molecule flavonoids. This encapsulation process holds potential for enhancing the solubility, permeability, and in vivo absorption of the flavonoids.

This study focuses on four representative flavonoids found in Astragali Radix, namely Calycosin-*7-O-β-D*-glucoside (CAG), Ononin (ON), Calycosin (CA) and Formononetin (FMN). This study represents the attempt to demonstrate the enhancement of the solubility, permeability and absorption of flavonoids by utilizing APS, and reveal the potential mechanisms as carriers of APS underlying the formation of multi-component co-delivery system resulting from interaction.

Materials and Methods

Materials

CAG, ON, CA and FMN (purity >98%) were purchased from Chengdu Pufei De Biotech Co., Ltd (Chengdu, China). Flavonoids (including CAG, ON, CA and FMN, with contents ≥74.8%) wXs prepared, and the remaining specimens were stored in our laboratory. APS (with contents ≥87.6%) was extracted and purified from the stem of Astragali Radix purchased from Anhui Huchuntang Chinese Medicine Decoction pieces Co., Ltd. (Anhui, China), following the methods described in our previous study.[18] Acetonitrile and methanol (UPLC grade) were obtained from Thermo Fisher Scientific. Egg yolk lecithin and dodecane were purchased from Shanghai Aladdin Biochemical Technology Co., Ltd., (Shanghai, China). Pepsin and trypsin are obtained from Sigma-Aldrich (UK). Phosphate, sodium hydroxide and hydrochloric acid were purchased from Guoyao Group Chemical Reagent Co., Ltd. All other reagents and chemicals were of analytical grade or higher quality.

Animals

Male Sprague-Dawley rats (250 ± 20 g) were obtained from Shanghai Jiesijie Laboratory Animal Co. Ltd. (Shanghai, China; SCXK (Hu) 2018–0004) and housed in a controlled environment (12 h light/dark cycles, 24 ± 2 °C, 55 ± 5% humidity) with ad libitum access to food and water. Rats were anesthetized with 2% pentobarbital sodium, intraperitoneally, at a dose of 0.3 mL/100 g. All animal experiments were approved by the Animal Ethics Committee of China Pharmaceutical University (2021–07-008) and performed in strict accordance with the national standards of the People's Republic of China, "Guidelines for Ethical Review of Laboratory Animal Welfare" (GB/T 35892–2018) and "Guidelines for the Review of Humane Endpoints in Animal Experiments" (RB/T 173–2018).

Molecular Dynamics (MD) Simulations

The GROMACS simulation package (version 2020.6) was utilized to perform atomistic MD simulations. The 2D molecular structure of flavonoids was sourced from the PubChem database (CID 137699082, 442813, 5280448, 5280378), and the gromos54a7 force field topology file for flavonoids was generated by the Automated force field Topology Builder website.[19,20] The 2D molecular structure of APS was obtained from the previous study.[21] The SPC water model was employed, and the GLYCAM_06j-1 force field was applied to model the polysaccharides. In the MD simulation, the LINCS algorithm was utilized to constrain all hydrogen atom bonds, and the Particle-mesh Ewald method was employed to calculate electrostatic interactions. The spatial position of the flavonoids was extracted, and the molecular van der Waals surface electrostatic potential was calculated using the Gaussian09 quantum chemistry comprehensive software package and the Multiwfn quantum chemistry wave function analysis program.[22,23] The simulation results were analyzed and visualized using the embedded programs in GROMACS and VMD1.9.4, and π-π stacking interactions were analyzed using the MD Analysis software package.

Characterization of Flavonoids-APS Complexes

Preparation of Flavonoids-APS Complexes

To prepare flavonoids-APS complexes, APS (80 mg) was dissolved in 20 mL water to obtain APS solution (4 mg/mL). Flavonoids (20 mg) was then dissolved in the APS solution (10 mL) and shaken in a constant temperature water bath at 37°C for 24 h. The mixture was then centrifuged at 12,000 r/min for 5 min, and the supernatant was freeze-dried to obtain the flavonoids-APS complexes.

Critical Aggregation Concentration (CAC) Determination

To determine the CAC, pyrene was used as a fluorescence probe. Namely, pyrene solutions (0.05 mL, 12×10^{-3} mg/mL in acetone) were added to a series of 10 mL brown test tube, and then the acetone was evaporated. Then, varying amounts of APS solutions (20 mg/mL in water) were added to each test tube and diluted with deionized water, resulting in a final APS concentration of 4, 2, 1, 0.5, 10^{-1}, 10^{-2}, 10^{-3}, 10^{-4} mg/mL. The solutions were shaken for 30 min before being placed in a 60 °C water bath for 3 h, cooled to 40 °C and then kept at constant temperature overnight. Fluorescence spectra of each solution cooled to room temperature were measured using a Shimadzu RF-5301 PC fluorescence spectrophotometer with an excitation wavelength of 335 nm and an emission range of 340–450 nm. The CAC value was determined by calculating the fluorescence intensity ratio of the first peak (I1, 373 nm) to the third peak (I3, 384 nm).

Dynamic Light Scattering (DLS)

The particle size and zeta potential of the flavonoids-APS complexes were determined by DLS (Zetasizer Nano-ZS90, Malvern, UK) after dissolving in deionized water (2 mg/mL).

Scanning Electron Microscopy (SEM)

The morphology and surface features of the freeze-dried flavonoids-APS complexes were observed and recorded using SEM (Regulus-8100, HITACHI, Tokyo, Japan) under high vacuum conditions.

Transmission Electron Microscope (TEM)

The microstructure of flavonoids-APS complexes was examined by TEM (H-7800, HITACHI, Tokyo, Japan). The samples were dissolved in ultrapure water, immediately dropped onto a 230-meter copper mesh, dried using infrared, stained with a drop of uranyl acetate solution for 10 min, and observed by TEM.

Characterization of Biopharmaceutical Properties

HPLC Analysis

The HPLC analysis was performed using a Waters 2695 system (Milford, MA, USA) with a photodiode array detector. CAG, ON, CA and FMN were separated on a Agilent Eclipse XDB-C_{18} column (4.6 mm × 250 mm, 5 μm) using a gradient elution of water (A) and acetonitrile (B). The gradient program was as follows: 0–2 min, 20%-23% B; 2–4 min, 23%-24% B; 4–5 min, 24–24% B; 5–8 min, 24–25%; 8–14 min, 25–33% B; 14–18 min, 35–100% B. The flow rate was set at 1.0 mL/min, and the column temperature was maintained at 30 °C. The detection wavelength was set at 254 nm, and the injection volume was 10 μL.

Chemical Stability

In vitro degradation studies were conducted to simulate the degradation in physiological environment. Artificial gastric juice, artificial small bowel fluid and artificial colon fluid were prepared according to Chinese Pharmacopoeia (2020). Flavonoids were incubated in buffer solutions with artificial gastric juice, artificial small bowel fluid and artificial colonic fluid at 37 °C to simulate the stomach, small intestine and large intestine. Flavonoids and APS weighed precisely according to the ratio of flavonoids: APS (1: 0, 1: 2, 1: 4, 1: 8, 1: 16) and added to the buffer solutions with different pH values. The samples were vortexed for 1 min, placed into a 37°C thermostatic oscillator (100 r/min), and collected at 0, 2, 4, 6, 8, 10, 12, 14.16 h for analysis using HPLC.

The degradation data were fitted to a first-order kinetic model, and the observed rate constants (k_{obs}) were obtained using equation (1). The one-tenth-life ($t_{0.9}$) and half-life ($t_{0.5}$) were also calculated from equation (2)-(3):

$$\mathrm{In}(C_t/C_0) = -k_{obs}t \tag{1}$$

$$t_{0.9} = 0.105/k_{obs} \tag{2}$$

$$t_{0.5} = 0.693/k_{obs} \tag{3}$$

where C_t and C_0 are the concentrations determined at various time points and the initial concentration, respectively.

Equilibrium Solubility

Phosphate buffer solutions with pH values ranging from 2.0 to 7.8 were prepared. CAG, ON, CA and FMN were added to 10 mL of each buffer solution. Ultrasound was utilized to ensure complete dissolution of the components, and the mixtures were then incubated in a constant temperature and oscillation shaker at 37°C and 120 r/min for 24 h until equilibrium was reached and saturation was achieved. The saturated solutions were treated with methanol, filtered through a 0.22 μm microporous membrane, and the subsequent filtrate was analyzed by HPLC to calculate the equilibrium solubility.

APS Solubilization

The solubility of flavonoids in the presence of APS was determined using the saturation shake-flask method. An excess amount of flavonoids was placed in a glass tube with a stopper, and 3 mL of distilled water were added. An appropriate

amount of APS was added to achieve a final concentration of 20 mg/mL. The mixtures were then incubated in a constant temperature and oscillation shaker at 37°C and 120 r/min for 24 h until equilibrium was reached and saturation was achieved. The saturated solutions were treated with methanol, filtered through a 0.22 μm microporous membrane, and the subsequent filtrate was analyzed by HPLC to calculate the solubility.

Oil-Water Distribution Coefficient (logP)

The logP of CAG, ON, CA and FMN was determined using the shake-flask method. The initial concentration (C_0) at distribution equilibrium of CAG, ON, CA and FMN was determined by adding flavonoids to 3 mL of water-saturated n-octanol solution (upper layer) until a large number of yellow insoluble precipitates appeared in the solution. Add APS according to the ratio of flavonoids:APS (1: 0, 1: 2, 1: 4, 1: 8, 1: 16). The solution was placed in a 37 °C thermostatic oscillator (100 r/min) for 24 h, and then centrifuged at 3000 r/min for 10 min. The supernatant was treated with methanol and analyzed by HPLC.

To determine the aqueous phase concentration (C_w) at distribution equilibrium of CAG, ON, CA and FMN, the drug-containing water-saturated n-octanol solution was absorbed, and the same amount of n-octanol-saturated buffer solution with different pH (1.2, 6.8, 8.3) was added. The solution was placed in a 37 °C thermostatic oscillator (100 r/min) for 24 h. The water phase was treated with methanol and analyzed by HPLC.

The logP was calculated with the following equation (4).

$$\mathrm{LogP} = \{\lg(C_o - C_w)/C_w\} \tag{4}$$

C_0-C_w is the concentration of the drug in n-octanol at equilibrium, and Cw is the concentration of the drug in the water at equilibrium.

Parallel Artificial Membrane Permeability Assay (PAMPA)

The PAMPA was conducted using a previously reported method with some technical modifications.[24] Paired glass permeable diffusion cells with a PVDF membrane sandwiched between them were divided into supply and receiving chambers. A 4% (w/v) n-dodecane solution of egg yolk lecithin (artificial membrane solution, 500 μL) was added to the PVDF membrane and allowed to equilibrate for 30 min. Donor solutions (8 mL) and drug solutions (2 mL) of flavonoids (30 mg/mL) and flavonoids-APS (flavonoids: APS=1: 2) were added to the receiving and supply chambers, respectively. The samples were placed in thermostatic oscillator (37 °C, 300 r/min) and collected at 2, 4, 6, 8, 10,12 h from the receiving chamber for analysis using HPLC.

Calculation of effective permeability coefficient (Lg_{Pe}) and effective transmittance (P_{eff}) according to equation (5), (6) and (7).

$$\mathrm{LgP_e} = \lg\{\frac{V_a V_d}{(V_a + V_d A \cdot t)} \cdot [-\ln(1 - \frac{[\mathrm{drug}]_a}{[\mathrm{drug}]_e})]\} \tag{5}$$

$$[\mathrm{drug}]_e = \frac{[\mathrm{drug}]_d \cdot V_d + [\mathrm{drug}]_a \cdot V_a}{V_d + V_a} \tag{6}$$

$$P_{eff} = \frac{[\mathrm{drug}]a}{[\mathrm{drug}]e} \cdot 100\% \tag{7}$$

V_d: volume of liquid added to the supply chamber; V_a: volume of liquid added to the receiving chamber; $A=\pi\text{-}r^2$: effective area of the artificial membrane; t: incubation time (s); $[drug]_a$: drug concentration in receiving chamber at time t; $[drug]_e$: theoretical equilibrium concentration at time t; $[drug]_d$: drug concentration in supply chamber at time t.

Rats in situ Single-Pass Intestinal Perfusion (SPIP) Model Studies

Eight 6-week-old male Sprague-Dawley rats, weighing 300–350 g, were fasted for 16 h with free access to water and randomly divided into two groups (n=4): the flavonoids group and flavonoids-APS group before the surgical procedures for SPIP, as previously described.[25] Random numbers were generated using the standard = RAND() function in Microsoft Excel. The rats were anesthetized with an intraperitoneal injection of 2% Pentobarbital sodium (0.3 mL/100 g) and placed under an infrared light to maintain a body temperature of 37°C. Four segments of the intestine (duodenum,

jejunum, ileum, and colon) were simultaneously perfused. The abdomen was opened with a 3–4 cm midline incision, and approximately 10 cm of the duodenum, jejunum, and ileum segment, and colon were exposed and cannulated on two ends with flexible PVC tubing.

For the flavonoids group, the flavonoids (CAG, ON, CA and FMN) were dissolved in Krebs-Ringer (K-R, 2 mg/mL) buffer. For the flavonoids-APS group, the flavonoids were dissolved in K-R buffer containing APS (4 mg/mL). The peristaltic pump (PetroGas Ausrüstgen, Berlin, Germany) was connected to the inlet, and the perfusate was collected at the outlet. The contents of the intestines were washed with pre-warmed saline, and saturated with K-R buffer for 15 min. A pre-warmed drug-containing perfusion solution was then perfused through the intestinal segment at a flow rate of 0.2 mL/min for 30 min to achieve a steady-state. Once the steady-state was reached, intestinal perfusate samples were collected at 15 min intervals for a total of 1.5 h, which were weighed before and after the perfusion. All samples, including the perfusion samples from both the inlet and outlet drug solutions at various time points, were immediately analyzed by HPLC.

At the end of the experiment, the lengths of the perfused intestinal segments were accurately measured. The effective permeability (P_{eff}) of drug was calculated using the following equations (8)-(9).

$$P_{eff} = \frac{-Q_{in}\ln\left(\frac{C_{out}}{C_{in}} \cdot \frac{V_{out}}{V_{in}}\right)}{2\pi rl} \tag{8}$$

$$K_a = \frac{\left(1 - \frac{C_{out}}{C_{in}} \cdot \frac{Q_{out}}{Q_{in}}\right)}{\pi r^2 l} Q_{in} \tag{9}$$

V_{in} and V_{out}: the volumes of the inlet and outlet; C_{in} and C_{out}: the concentrations of the perfusate at the inlet and outlet; Q_{in}: the flow rate of the perfusion; l and r: the length (cm) and radius (cm) of the perfused intestinal segment.

In vivo Pharmacokinetics Study

Experimental Design

Male Sprague-Dawley rats weighing 250–300 g were subjected to a 12 h fasting period with ad libitum access to water before being randomly divided into two groups (n=6): the flavonoids group and the flavonoids-APS group. In the flavonoids group, the flavonoids were dissolved in water at a concentration of 10 mg/mL, while in the flavonoids-APS group, the flavonoids were dissolved in APS solution at a concentration of 20 mg/mL. Both groups of rats were orally administered their respective solutions at an equivalent dose. Following administration, plasma samples were collected at predetermined time intervals (0, 5, 15, 30, 45, 60, 120, 180, 240, 360, 480 and 720 min) via orbital blood collection under anesthesia. Anesthesia was induced by intraperitoneal injection of 2% pentobarbital sodium at a dose of 0.3 mL/100 g. The collected blood samples were subsequently centrifuged at 3000 r/min for 10 min at 4 °C, resulting in approximately 150 μL of plasma samples. These samples were then stored at −80 °C until further analysis using LC-MS/MS.

Pre-Treatment of the Plasma Samples

In plasma sample preparation, 100 μL plasma sample was spiked with 10 μL baohuoside II (IS) solution, 10 μL hydrochloric acid (3 M), and 500 μL acetonitrile. The mixture was then vortexed for 3 min. After centrifugation at 13,000 r/min for 5 min, the supernatant was dried using a vacuum centrifugal concentrator (Labconco CentriVap, Kansas, USA). The dried sample was then dissolved, centrifuged once again, and subsequently injected into the high-performance liquid chromatography-mass spectrometry (LC-MS/MS) system. The pharmacokinetic parameters were calculated using Drug and Statistics version 1.0.

High Performance Liquid Chromatography-Mass Spectrometry Analysis

LC-MS/MS analysis was performed using an Agilent system equipped with ACQUITY UPLC® BEH C18 column (2.1 mm × 50 mm, 1.7 μm), maintained at 30 °C. The mobile phase consisted of water (A) and acetonitrile (B). The gradient program was

performed as follows: 0–1.0 min, 10% B; 1.0–2.0 min, 10%–50% B; 2.0–5.0 min, 50%–55% B; 5.0–5.2 min, 55–95% B; 5.2–9.5 min, 95–100% B. The flow rate was set at 0.3 mL/min, and the injected volume was 3 μL.

Mass analysis was carried out using a 6420 Triple Quad LC/MS system equipped with an electrospray ionization source. Multiple reaction monitoring was utilized in positive and negative modes with the following MS settings: gas temperature of 350 °C, gas flow rate of 12 L/min, nebulizer pressure of 35 psi, capillar voltage of 4000 V, fragmentor voltage of 135V, collision voltage of 30V, and transitions of m/z 477.0/285.0 for CAG, m/z 431.0/269.0 for ON, m/z 283.0/211.0 for CA, m/z 267.0/222.9 for FMN, m/z 499.0/280.9 for IS.

Method Validation

Validation was carried out according to the USA Food and Drug Administration Bio-analytical Method Validation Guidance, including determination of the selectivity, calibration curve, precision, accuracy, stability, matrix effect and recovery.[26]

Multi-Spectroscopy Exploration

X-Ray Diffraction (XRD)

The XRD patterns of flavonoids, APS and flavonoids-APS complexes were obtained using a Bruker D8 Advance X-ray diffractometer with Cu-Ka radiation (λ = 1.54056Å) radiation. The scanning range for all samples was from 2θ angle 3° to 80°.

Thermogravimetric Analysis (TGA) and Differential Scanning Calorimetry (DSC)

The thermal behaviors of flavonoids, APS and flavonoids-APS complexes were analyzed using a TGA analyzer (PerkinElmer TGA 4000, Llantrisant, Wales, UK) and DSC analyzer (DSC, Netzsch DSC 3500, Germany). The experimental conditions were as follows: dynamic nitrogen atmosphere (99.999%), heating rate of 20 °C/min from 30 to 500 °C, with a sample mass of approximately 4 mg.

Fourier-Transform Infrared (FT-IR) Spectroscopy

The FT-IR spectra of flavonoids, APS and flavonoids-APS complexes were studied using FT-IR spectroscopy (Bruker Tensor 27 FT-IR Spectrometer). The samples were analyzed directly in powder form without the use of KBr. The range of spectrophotometer was from 400 cm^{-1} to 4000 cm^{-1}.

Statistical Analysis

One-way analysis of variance (ANOVA) or two-sided Student's *t*-test was performed using Origin Pro 2022 software (OriginPro Software, Inc., Northampton, Massachusetts, USA) to assess significant differences between the groups, and the results were expressed as mean ± standard deviation (SD). Differences were statistically significant when $P<0.05$.

Results and Discussion

Self-Assembly Properties and Biopharmaceutical Properties of Flavonoids

Self-Assembly Properties of Flavonoids

The present study investigated the self-assembly behavior of CAG, ON, CA and FMN (Figure 1A), in a water-soluble system of 10×10×10 nm using molecular dynamics simulation for a duration of 40 ns. The simulation trajectory demonstrated that CAG, ON, CA and FMN can spontaneously form cluster states (Figure 1B). The simulation data analysis revealed that the long-range electrostatic force (Coulomb-14) is the driving force for the self-assembly of the CAG, ON, CA and FMN (Figure 1C and D), and hydrogen bond and π-π stacking with CAG and ON also play an important role in the self-assembly (Figure 1E-H). The solvent-accessible surface area (SASA-Area) decreases (Figure 1G), indicating the presence of stable self-assembled nanostructures in the water-soluble system. Moreover, the solvation free energy (Solvation-Gsolv) decreases (Figure 1G), indicating that CAG, ON, CA and FMN are more soluble in water after self-assembly, suggesting that the self-assembly behavior of CAG, ON, CA and FMN is beneficial to their solubility in water to some extent. Studies have discovered that a variety of active components, such as flavonoids, alkaloids, glycosides, terpenoids, organic acids and metal ions tend to form self-assembled nanoparticles at micromolar concentrations under water-rich conditions.[27–29] The interaction

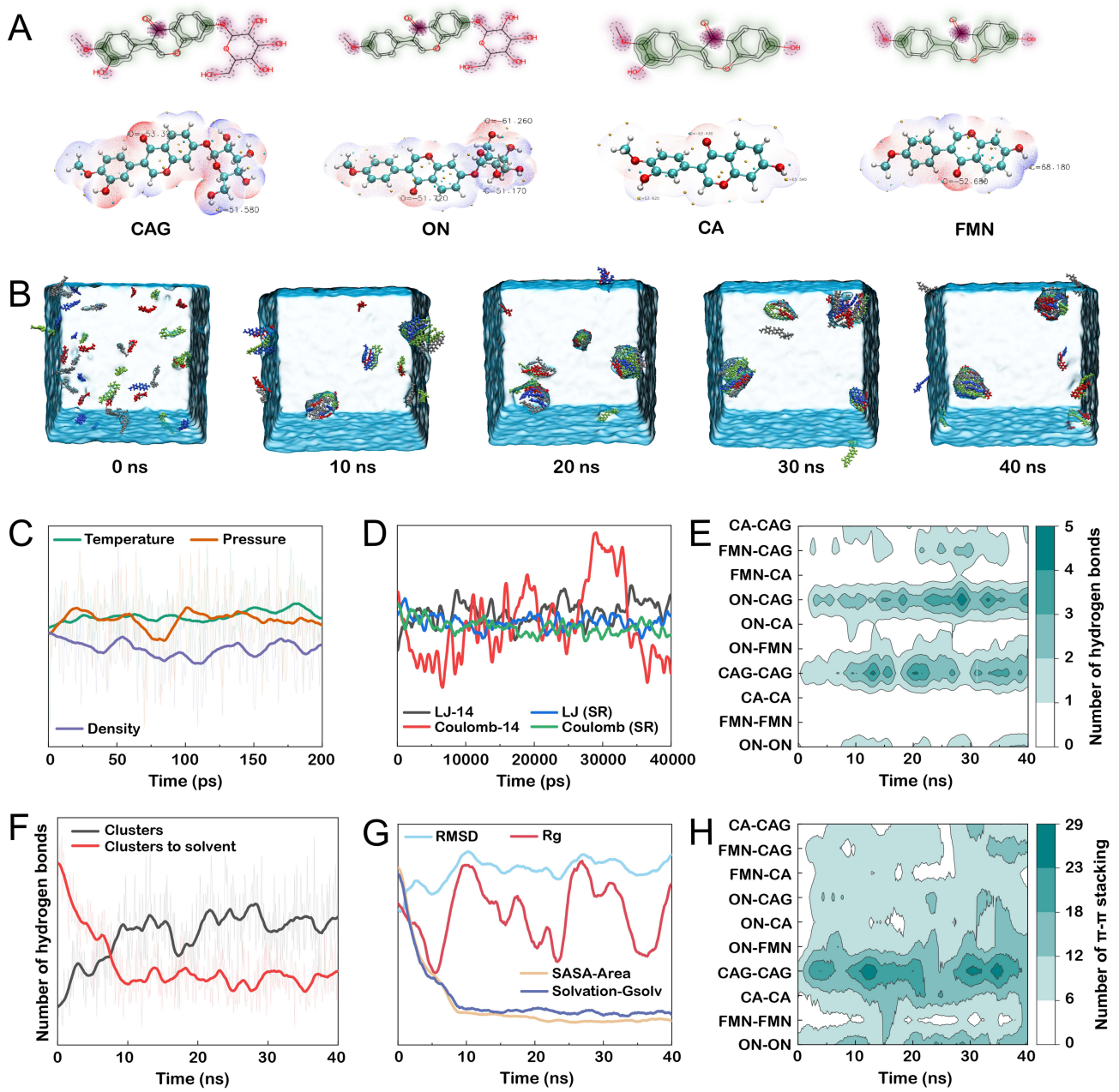

Figure 1 The molecular simulation trajectory and data analysis of CAG, ON, CA and FMN in aqueous solution. (**A**) The van der Waals surface electrostatic potential of CAG, ON, CA and FMN, red represents positive potential, blue represents negative potential, yellow balls corresponding maximum potential points, and cyan balls corresponding minimum potential points; (**B**) Simulation trajectory of CAG, ON, CA and FMN in aqueous solution system from 0 to 40 ns; (**C**) The temperature, pressure and density of the equilibrium system; (**D**) The changes in different types of interaction forces in the molecular simulation system; van der Waals force (LJ), Coulomb, short-range (SR), long-range (14); (**E**) The number of intermolecular hydrogen bonds of components (defined as hydrogen bonds if the distance between donor and recipient is less than 4.0 and the corresponding angle is greater than 120°); (**F**) The number of intermolecular hydrogen bonds of components, and intermolecular hydrogen bonds of components and water molecules; (**G**) Root-mean-square deviation (RMSD), gyration radius (Rg), SASA-Area and Solvation-Gsolv; (**H**) The number of π-π stacking interactions between components.

between components in self-assembled nanoparticles has been found to enhance solubility, permeability and absorption.[30] This discovery has prompted a shift in focus from studying individual components to examining their interactions.

Characterization of Solubility and Permeability of Flavonoids

It is widely acknowledged in the scientific community that a component's water solubility is considered favorable when its equilibrium solubility exceeds 0.1 mg/mL, as solubilities below 0.1 mg/mL often exhibit dissolution-dependent

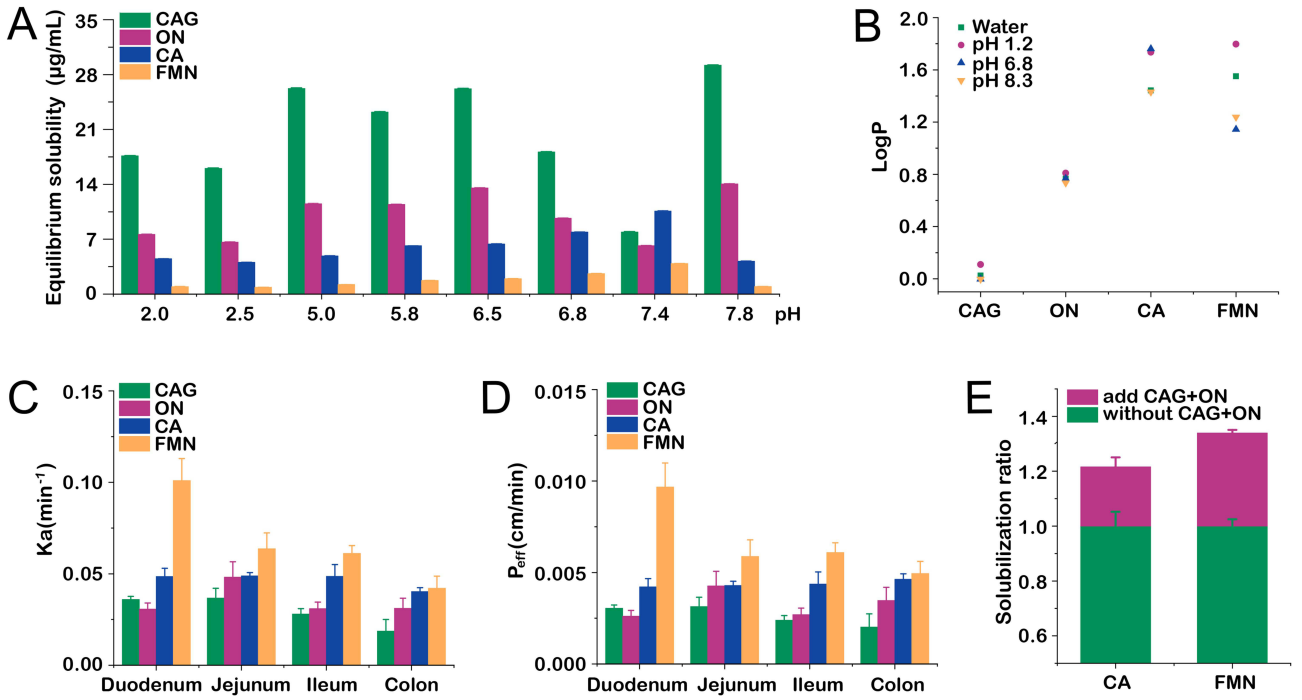

Figure 2 The solubility and permeability of CAG, ON, CA and FMN. (**A**) The equilibrium solubility of CAG, ON, CA and FMN; (**B**) The logP value of flavonoids at water and pH 1.2, 6.8 and 8.3; (**C**) The *Ka* of flavonoids measured by SPIP; (**D**) The P_{eff} of flavonoids measured by SPIP; (**E**) The phenomenon of increased solubility of CA and FMN in CAG and ON aqueous solution. Compared with flavonoids.

absorption.[31–33] The equilibrium solubility of the CAG, ON, CA and FMN were below 30 μg/mL (Figure 2A), indicating that CAG, ON, CA and FMN are low-solubility components. The logP value, which reflects the distribution of a component in the oil and water phases, is a predictor of permeability. A higher logP value implies greater lipophilicity, while a lower logP value suggests greater hydrophilicity. A component with a logP < 1 is considered to have poor permeability and is difficult to penetrate the interior of cells via biological membranes, while a component with a 2 < logP < 3 is considered to have good permeability.[34–36] The logP < 1 of CAG and ON indicating poor permeability, while the 1 < logP < 2 of CA and FMN, suggesting greater permeability than CAG and ON but still not ideal (Figure 2B). The results of in vivo intestinal perfusion in rats (Figure 2C and D) confirm the above findings. The research results indicate that CAG, ON, CA and FMN all exhibit varying degrees of solubility and permeability issues. However, it is interesting to note that with the joint participation CAG and ON, the solubility of CA and FMN can be increased by 1.22-fold and 1.34-fold respectively (Figure 2E), which is consistent with the results of molecular dynamics simulation, indicating that CAG and ON can enhance the solubility of CA and FMN. Besides, these findings are consistent with several previous numerous studies that have demonstrated that the nanoaggregates formed by self-assembly of multiple components have the effect of increasing component stability and solubility.[37–39]

APS Can Serve as Natural Carriers Using Self-Assembly Properties

APS is a type of polysaccharide with a complex branched structure. In this study, the behavior of APS in aqueous solution was simulated (Figure 3A) based on the previously reported structure of APS.[21] Molecular dynamics simulation (40 ns) was performed on an aqueous solution system after the random insertion of five APS molecules. The simulation results demonstrate that APS can undergo self-assembly to form cluster states and aggregate structures (Figure 3C). The decrease in SASA-Area also indicates that the system has a stable self-assembled nanostructure (Figure 3B). Overall, these findings suggest that APS exhibits a stable self-assembled nanostructure in aqueous solutions.

Self-assembly refers to the spontaneous organization or aggregation of molecules into stable structures, driven by non-covalent interactions.[40] APS is a macromolecular polysaccharide with branched chains and a unique structure, which has the ability to self-assemble to form aggregates. The resulting aggregates formed by the self-assembly of APS exhibit

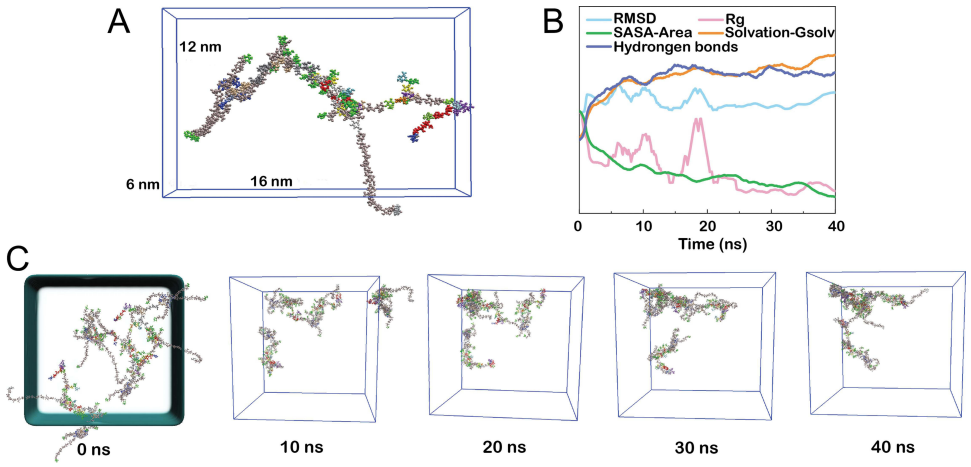

Figure 3 The molecular simulation trajectory and data analysis of APS in aqueous solution. (**A**) Structural model of APS; (**B**) Data analysis of simulation process, including RMSD, Rg, SASA-Area, Solvation-Gsolv, the number of hydrogen bonds of APS (defined as hydrogen bonds if the distance between donor and acceptor is less than 4.0 and the corresponding angle is greater than 120°); (**C**) Simulation trajectory of APS in aqueous solution system from 0 to 40 ns.

a porous structure and a large surface area, which suggests their potential value as carriers with larger drug loading capacity. Natural polysaccharides are green alternatives for designing biopolymeric nanoparticles as suitable nanocarriers due to their amphiphilic nature compatible with many bioactives and unique functional properties. Moreover, the self-assembly of natural polysaccharides represents a green approach to self-assembly, as it does not require the addition of exogenous components. This eco-friendly method reduces the potential for harmful toxic cross-linking in biomedical applications.[41] The utilization of natural polysaccharides in design of micro/nanoparticulate systems highly attractive due to their well-established properties. Various polysaccharides, such as chitosan, alginate, guar gum, starch, pectin, hyaluronic acid and xanthan gum, have been extensively employed in micro- and nanoparticulate systems for oral colon-targeted drug delivery.[42,43]

Microstructure of Flavonoids-APS Complexes

CMC Determination

In the aqueous solution of flavonoids, APS and flavonoids-APS complexes, the Tyndall effect was observed (Figure 4A). This observation indicates that in addition to the formation of flavonoids-APS complexes, there is also a presence of multi-component self-assembly in solution systems of flavonoids and APS. These findings are consistent with the results obtained from MD simulation. The CMC of APS was determined using pyrene fluorescence as a probe to validate this. As illustrated in Figure 4B, two straight lines were produced (Y=−0.00344X+1.246, Y=−0.2227X+1.180), and the CMC was calculated as 0.499 mg/mL from the intersection point of Y1 and Y2.

Size, PDI and Zeta Potential

The DLS was employed to investigate the size of flavonoids-APS complexes formed by the combination of flavonoids and APS. The results demonstrated that the average size of flavonoids-APS complexes was significantly larger than that of the flavonoids alone, but much smaller than APS. The average size of the complexes was found to be in the range of 200–300 nm (Figure 4C and D). When the ratio of APS to flavonoids was ≤4, the polydispersity index (PDI) remained below 0.2. (Figure 4E). The zeta potential of flavonoids-APS complexes was slightly lower than that of flavonoids alone but remained relatively stable (Figure 4F). These findings indicate that flavonoids can integrate with APS, forming evenly distributed and stable flavonoids-APS complexes.

TEM Analysis

The morphology of the flavonoids-APS complexes was further investigated using TEM, and representative images were presented in Figure 4G. Based on the TEM images, the particle sizes of the flavonoids-APS complexes were estimated to be in the range of 200–300 nm, exhibiting a spherical shape and well-defined contours. The TEM analysis results were

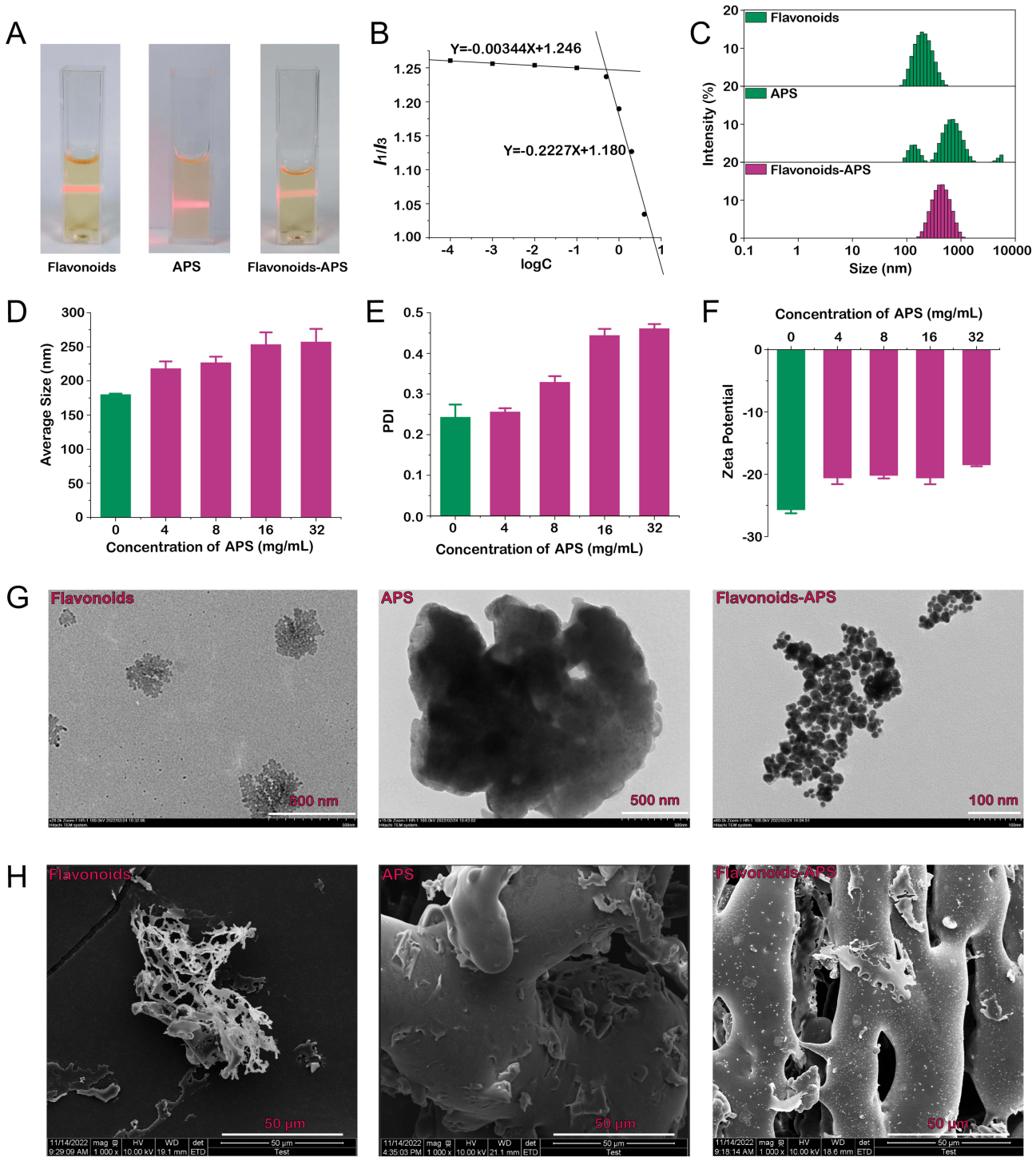

Figure 4 Microstructure of flavonoids-APS complexes. (**A**) Tyndall phenomenon of flavonoids, APS and flavonoids-APS complexes; (**B**) The CMC of flavonoids-APS complexes; (**C**) Particle size comparison among flavonoids, APS and flavonoids-APS complexes; (**D**) Average size; (**E**) PDI; (**F**) Zeta potential; (**G**) TEM; (**H**) SEM (×1000).

consistent with MD simulations, which indicated that flavonoids can self-assemble to form nanoparticles with sizes ranging from 100–200 nm. However, due to the large molecular weight of APS, it tends to form micron-sized particles during self-assembly. Nevertheless, upon interacting with flavonoids, the particle size decreases, forming flavonoids-APS complexes with well-defined contours and a multi-spherical shape, ranging from 200 to 300 nm in size.

SEM Analysis

To investigate the morphological changes of flavonoids-APS complexes, SEM was utilized to observe the surface morphology of flavonoids-APS complexes. The results, presented in Figure 4H, reveal that the self-assembled nanoparticles of flavonoids exhibited hollow structures and were arranged in lamellar aggregates. On the other hand, APS appeared as stout branches. In contrast to flavonoids and APS, the surface of flavonoids-APS complexes exhibited more holes and attached lamellar nanoparticles. This observation suggests that flavonoids may have been adsorbed on the surface or encapsulated within APS during the self-assembly process. Numerous studies have consistently demonstrated that polysaccharides, proteins, and small molecule active components readily interact to form nanoparticles with sizes ranging from 200 to 400 nanometers and exhibiting loading properties.[44]

APS Improve the Biopharmaceutical Properties of Flavonoids

APS Enhance the Chemical Stability of Flavonoids

The chemical stability of the components in vivo plays a vital role in their absorption. The degradation kinetics curves presented in Figure 5 demonstrate that the degradation of CAG, ON, CA and FMN follows first-order kinetics at different pH values, regardless of whether they are combined with APS or not. The degradation kinetics curves and corresponding parameters, including k_{obs}, correlation coefficient (r), $t_{0.9}$ and $t_{0.5}$, are listed in Table S1. The experimental findings indicate that the combination with APS significantly enhances the chemical stability of CAG, ON, CA and FMN in simulated stomach, small intestine and colon. In artificial gastric juice, the $t_{1/2}$ of CAG, ON, CA and FMN combined with APS were 1.08–2.61 fold, 1.03–1.82 fold, 1.03–5.15 fold and 1.03–4.36 fold, respectively, compared to when they were administered alone. Premature degradation of active components in the upper gastrointestinal tract is a crucial factor that affects the efficacy of drugs. Upon formation of flavonoids-APS complexes, the hydrophilic properties of most polysaccharides causes them to distribute on the surface of the complex, thereby reducing the degradation of flavonoids to some extent. Presently, numerous studies have indicated that self-assembly or encapsulation of active components in nanoparticles can effectively protect them from premature degradation in the stomach and small intestine, leading to enhanced stability.[45,46] These findings align with the results obtained in this study.

APS Enhance the Aqueous Solubilities of Flavonoids

The addition of APS considerably increased the aqueous solubility of CAG, ON, CA and FMN by approximately 1.39-fold, 1.44-fold, 1.80-fold and 2.05-fold, respectively, compared to the solubilities of the flavonoids alone (Figure 6A and B). These findings suggest that APS significantly improved the aqueous solubilities of the flavonoids, in line with previous research that have reported the ability of polysaccharides to improve the solubility of hydrophobic components.[10] The enhanced solubility may be attributed to the formation of complexes or interactions between APS and the flavonoids, which may contribute to an increased dissolution rate and solubility of the flavonoids. Additionally, the amphiphilic nature polysaccharides, such as APS, can aid in solubilizing hydrophobic components by forming a hydrophilic shell around the molecules, thus improving their aqueous solubility.[47]

APS Improve the Permeability of Flavonoids

APS can intervene in the distribution of flavonoids (CAG, ON, CA and FMN) in octanol (oil) and water, and its distribution is greatly affected by pH (Figure 6C-F). After combined with APS, the logP values of CAG, ON, CA and FMN were changed to varying degrees, among which APS can significantly increase the distribution of FMN in oil, indicating that APS may play an important role in promoting the permeation and absorption of FMN.

PAMPA has become an increasingly popular in vitro method for predicting passive intestinal absorption over the past few decades. It serves as a complementary and alternative approach to the Caco-2 assay in pharmaceutical research. In our study, we found that the permeability of flavonoid glycosides (CAG and ON) was significantly lower than that of flavonoid aglycones (CA and FMN), as shown in Figure 7A. This difference in permeability could be attributed to the fact that glycosylation of flavonoids can reduce their lipophilicity, which subsequently leads to a decreased passive diffusion across the lipid bilayer. Interestingly, our findings indicated that APS had a greater influence on the permeability of CAG, ON, and CA compared to FMN. This suggested that APS might have a role in modulating the

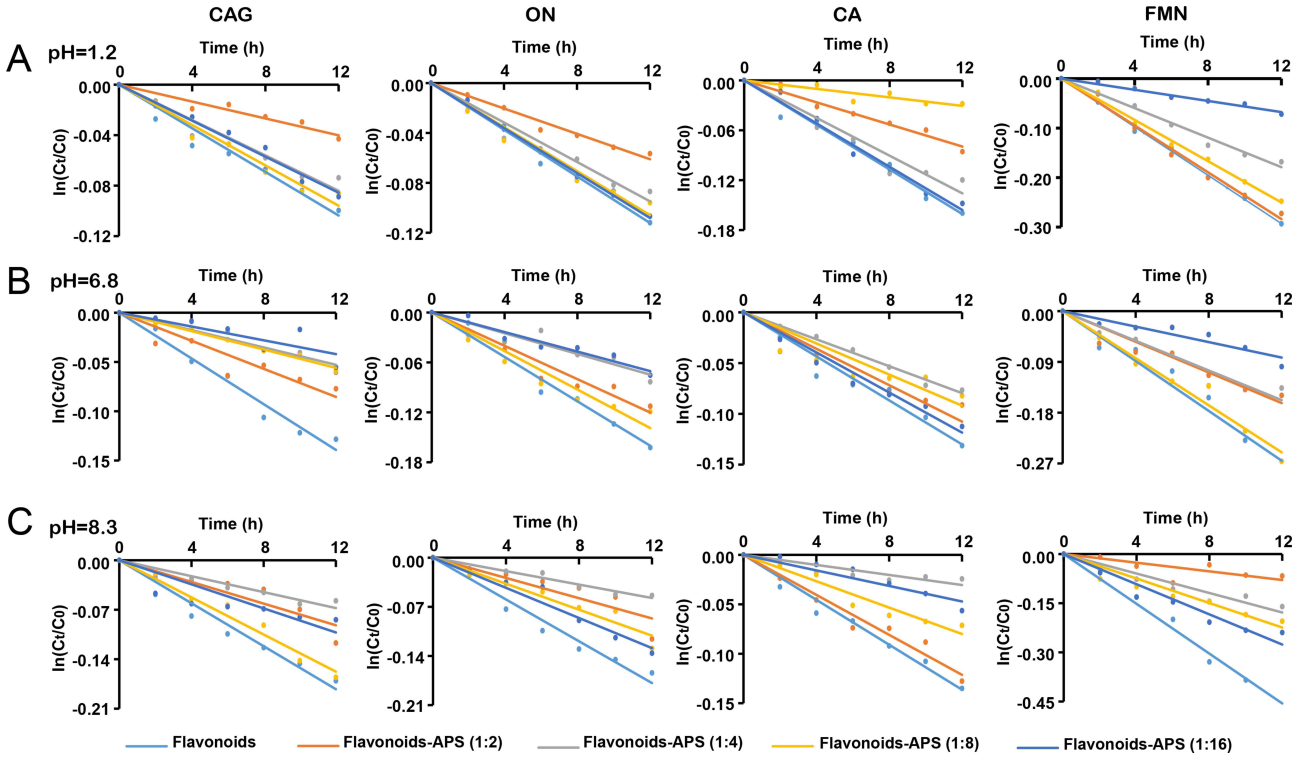

Figure 5 The relationship between $\ln(C_t/C_0)$ for flavonoids in aqueous and saturated APS solution under accelerated degradation conditions. (**A**) Artificial gastric juice; (**B**) Artificial small bowel fluid; (**C**) Artificial colonic fluid.

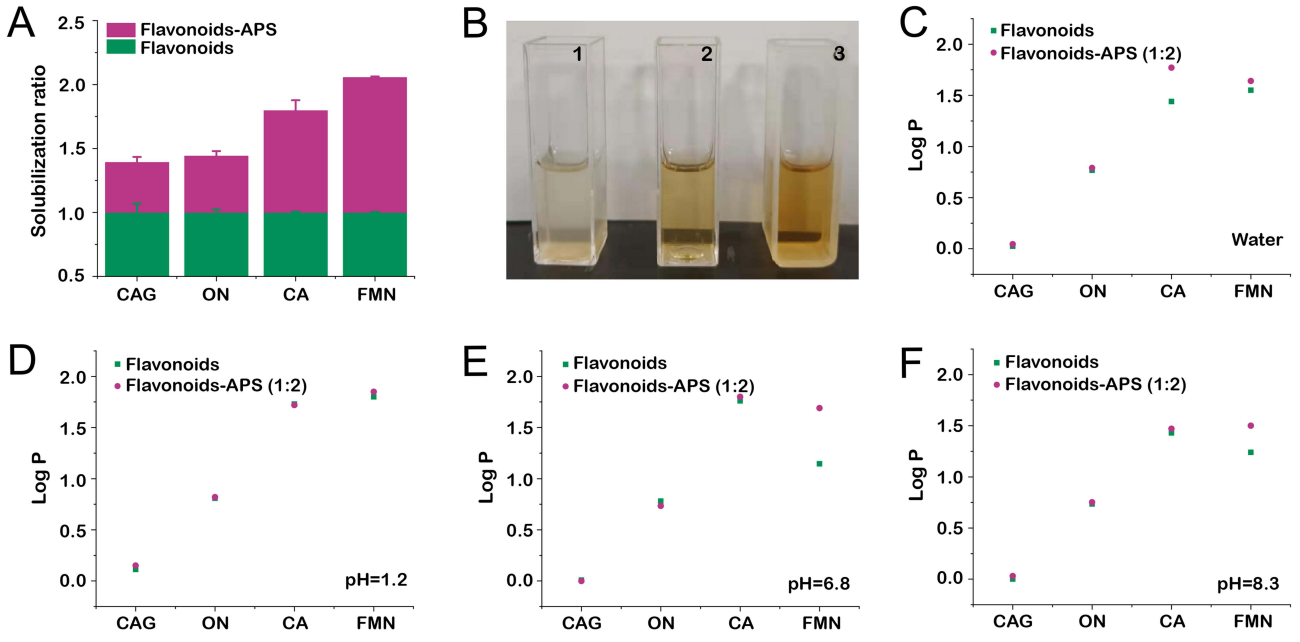

Figure 6 The effect of APS aqueous solution on the solubility and logP of flavonoids. (**A**) The solubilization ratio of CAG, ON, CA and FMN in APS aqueous solution; (**B**) The phenomenon of increased solubility of flavonoids in APS aqueous solution (1: flavonoids, 2: flavonoids-APS, APS); (**C-F**) The influence of APS on the logP value of flavonoids at water and pH 1.2, 6.8 and 8.3.

interactions between flavonoids and the lipid membrane, potentially by modifying the physicochemical properties of the membrane or by forming complexes with flavonoids that aid in their permeation.

To investigate the effect of APS on the intestinal absorption of flavonoids, the intestinal mucosal permeability experiment in rats using the SPIP technique. The permeability of CAG, ON, CA and FMN was measured individually

and in combination with APS, as shown in Figure 7B and C. The absorption rate constant (Ka) and effective permeability (P_{eff}) values indicated that the jejunum exhibited the absorption efficiency for CAG and ON, while the colon showed optimal absorption for CA, and the duodenum was the primary site for FMN absorption. Additionally, APS was observed to increase the intestinal mucosal permeability of flavonoids across different segments of the intestines, with a more significant impact observed in the most efficient absorption segment (n=4). These findings suggested that APS could serve as an oral drug carrier, enhancing the oral bioavailability of flavonoids by improving intestinal mucosal permeability in both the small and large intestines.

The gelatinous substance known as the mucus layer the intestinal epithelium, providing protection against the invasion of pathogens and toxins by hindering their adhesion and penetration into the mucosal epithelial cells. However, this mucus layer can also hinder the penetration and absorption of orally administered drugs, leading to reduced bioavailability.[48,49] The enhanced permeability of flavonoids in the presence of APS can be attributed to the hydrophilic properties of APS, which provides a favorable environment for the crossing of the mucus layer (Figure 8). These findings indicated that APS could serve as a permeability enhancer or "excipient", altering the barrier function of the intestinal epithelium. In addition, gaining a better understanding of the role of APS in promoting the penetration and absorption of flavonoids could contribute to the development of novel strategies to optimize the therapeutic potential of flavonoids, particularly when their bioavailability is a limiting factor.

APS Improve the Pharmacokinetics of Flavonoids

The pharmacokinetics of flavonoids, including CAG, ON, CA and FMN, were assessed following oral administration of both individual flavonoids and flavonoids-APS combinations (at equivalent doses). The plasma concentration–time curves are depicted in Figure 9. Various pharmacokinetics parameters, including maximum concentration (C_{max}), area under the concentration–time curve (AUC), half-time ($t_{1/2}$) and elimination rate constant (K_e), were calculated and presented in Table S2. These findings highlight the notable distinctions in the pharmacokinetics of flavonoids when administered alone, compared to their combination with APS (n=6).

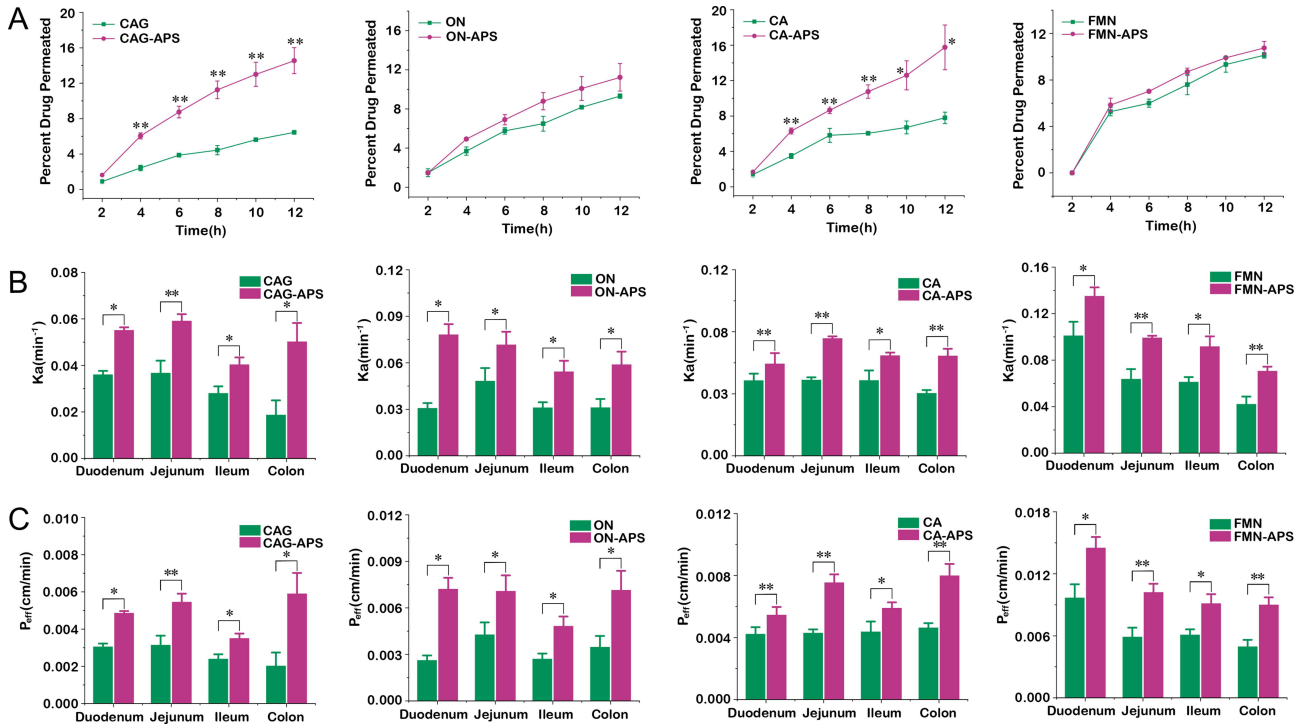

Figure 7 The improvement effect of APS on the permeability of flavonoids. (**A**) The permeability of flavonoids measured by PAMPA; (**B**) The Ka of flavonoids measured by SPIP; (**C**) The P_{eff} of flavonoids measured by SPIP. Compared with flavonoids, *$P < 0.05$; **$P < 0.01$.

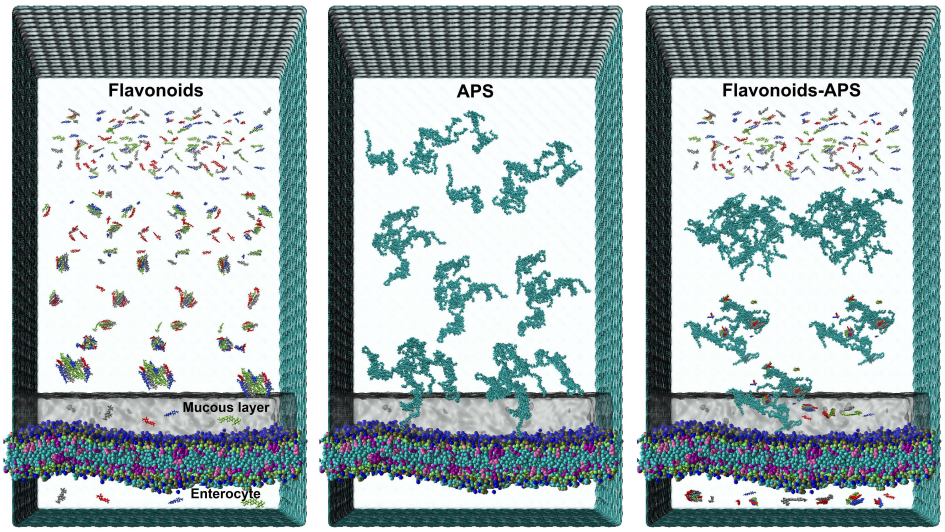

Figure 8 Diagram illustrating the enhanced permeability of flavonoids facilitated by APS. APS can provide a favorable environment for mucosal penetration, enhancing the permeability of flavonoids.

The pharmacokinetic investigation revealed that APS significantly enhanced C_{max}, area under the concentration–time curve from 0 to the last measurable time point (AUC_{0-t}) and area under the concentration–time curve from 0 to infinity ($AUC_{0-\infty}$) of CA and FMN, compared to their administration as individual flavonoids. Furthermore, APS notably increased the $t_{1/2}$ of CA, indicating a reduction in its elimination rate. These results suggested that APS could improve the bioavailability of CA and FMN, thereby enhancing their therapeutic effects. Similarly, APS demonstrated a significant improvement in the C_{max} ($P < 0.05$ or $P < 0.01$) of CAG and ON, suggesting that these flavonoids could exert their medicinal effects more intensely when combined with APS. This observation supports previous research suggesting that the combination of flavonoids with polysaccharides could lead to an enhanced efficacy.[50]

In addition, studies have indicated that the absorption of active components is associated with the formation of nanoparticles. For instance, nanoparticles of *Coptidis Rhizoma* (Huang lian) polysaccharide can enhance the absorption of the active components berberine in the intestine, and the mechanism may be related to the regulation of tight junctions between intestinal epithelial cells.[51] Additionally, the validation results for selectivity, calibration curve, precision, accuracy, stability, matrix effect and recovery are presented in Table S3-S6.

The Mechanism of Flavonoids-APS Complexes Formation

XRD

The XRD patterns provide insight into the crystallinity and structural properties of flavonoids, APS and flavonoids-APS complexes are displayed in Figure 10A. The broad diffraction peaks observed for both flavonoids and APS indicate relatively low crystallinity. This observation is consistent with previous research on flavonoids and polysaccharides, which often exhibit low crystallinity due to their complex molecular structures and hydrogen bonding networks.[52] Interestingly, the XRD patterns of the flavonoids-APS complexes did not exhibit significant changes compared to the individual components. This implies that the crystal structure of the flavonoids-APS complexes did not undergo a major alterations. This finding suggests that the interaction between flavonoids and APS is primarily driven by non-covalent forces, such as hydrogen bonding or LJ, rather than significant modifications in the crystal structure. This discovery is consistent with the previous research of flavonoids and other macromolecular components.[53]

TGA and DSC

The TG-DSC curves presented in Figure 10B offer valuable insights into the thermal stability and heat uptake changes of flavonoids, APS and flavonoids-APS complexes. The weight loss curve exhibits three primary steps, corresponding to the loss of free and combined water, degradation of the sugar chains, and reorganization process. The TG analysis shows that

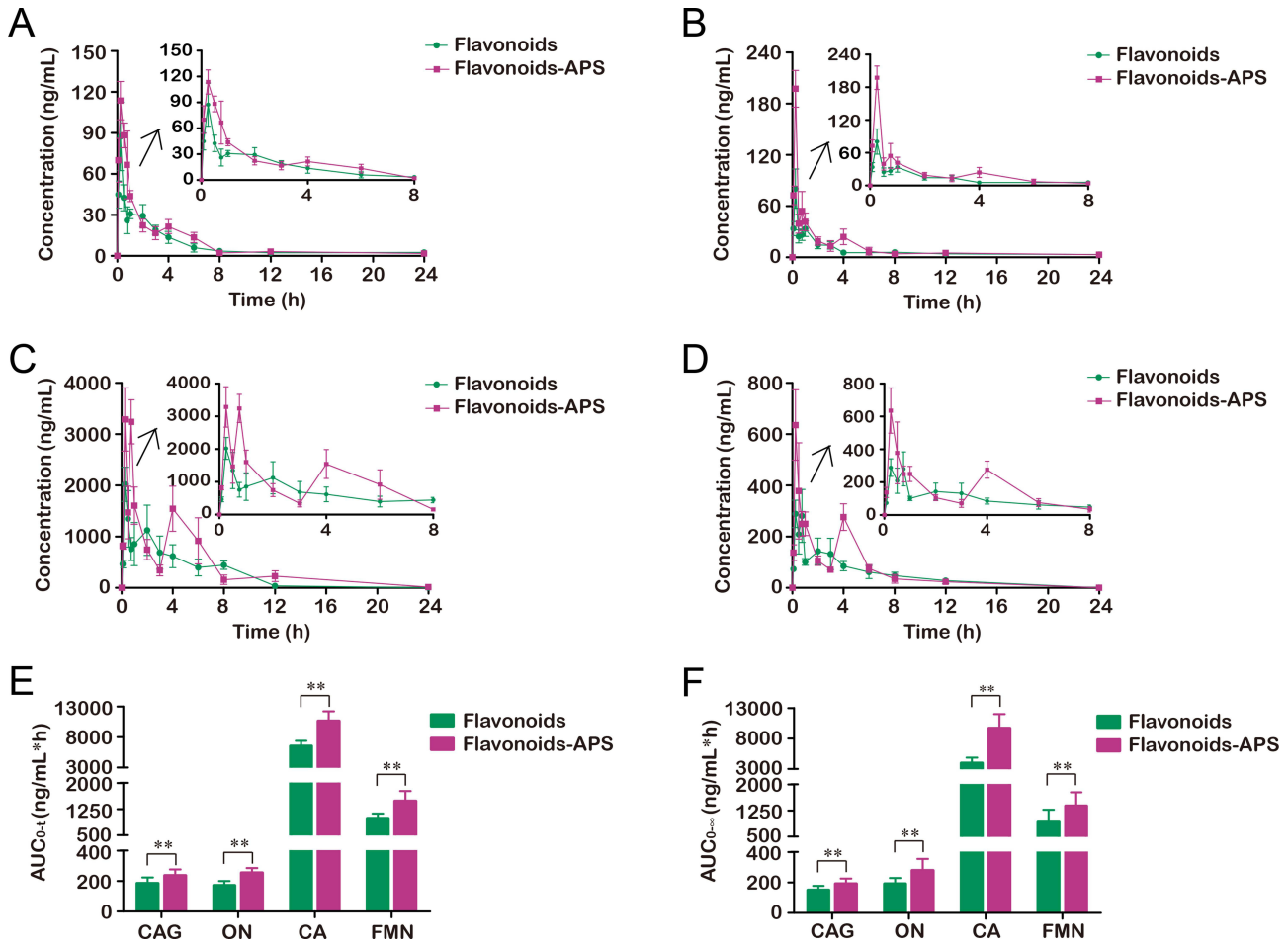

Figure 9 Plasma concentration-time curves of flavonoids. (**A**) CAG, (**B**) ON, (**C**) CA, (**D**) FMN, (**E**) AUC_{0-t}, (**F**) $AUC_{0-\infty}$. Compared with flavonoids, $^{**}P < 0.01$.

the mass loss of flavonoids-APS complexes between 35°C and 480°C is 60.53%. In comparison, the mass loss of flavonoids alone within the same temperature range is 63.36%. This suggests that the flavonoids-APS complexes exhibit improved thermal stability in contrast to the flavonoids alone. This improvement in thermal stability can be attributed to the interactions between flavonoids and APS, which stabilize the overall structure and confer resistance to thermal degradation.

The DSC analysis provides further evidence supporting the hypothesis of structural changes in flavonoids upon complex formation with APS. The distinct heat absorption peaks of flavonoids (100–130°C) and flavonoids-APS complexes (130–160°C) indicate that the structure of flavonoids has been altered after forming complexes with APS. This divergence in thermal behavior suggests that the interactions between flavonoids and APS induce modifications in the structure of flavonoids, thereby influencing their thermal properties and transition temperature. These findings hold significant importance in the design and development of novel drug formulations and delivery systems that utilize flavonoids and APS. Understanding the thermal stability and structural changes of these complexes is crucial for optimizing their performance and stability under various conditions.

The glass transition temperature (Tg) is a critical parameter that characterizes the thermal stability and structural properties of materials, and is influenced by the amorphous degree and crystalline nature of polymers. High Tg values generally indicate greater crystallinity and low amorphous content, providing structural stability and resistance to high temperatures. The crystallization temperature (Tc) is another crucial parameter that describes the thermal properties and structural characteristics of materials, particularly polymers. Tc represents the temperature at which a polymer transitions

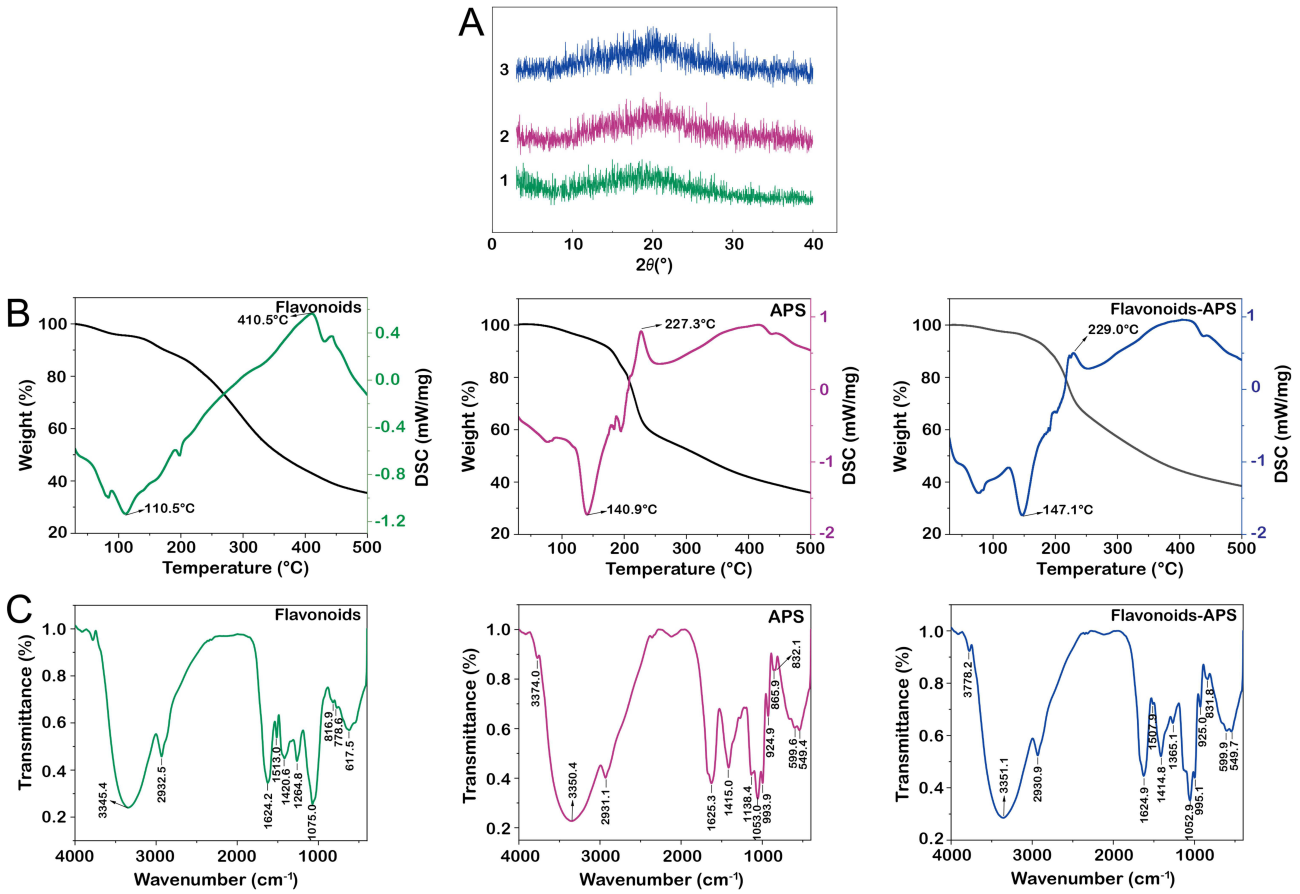

Figure 10 Multi-spectroscopy exploration of flavonoids, APS and flavonoids-APS complexes. (**A**) XRD patterns; (**B**) TG-DSC curves; (**C**) FT-IR spectra.

from its amorphous or disordered state to a crystalline state upon cooling. A higher Tc signifies improved structural organization and stronger intermolecular forces, contributing to the overall stability and performance of material.

In the case of flavonoids-APS complexes presented in Figure 10B, the increase in both Tg and Tc values suggests that the complexes exhibit higher thermal stability and structural rigidity compared to the flavonoids alone. The improvement in thermal stability could be attributed to the formation of intermolecular bonds between flavonoids and APS, which provide enhanced structural support and restrict the mobility of the molecular chains. These findings align with the results obtained from the TGA analysis, further reinforcing the idea that flavonoids-APS complexes possess greater thermal stability compared to their individual components.

FT-IR Spectra

The FT-IR spectra analysis of flavonoids, APS and flavonoids-APS complexes are shown in Figure 10C. The FT-IR spectra of flavonoids exhibited various typical absorption bands. These include the carbohydrate hydroxyl "-OH" band at 3345 cm^{-1}, the conjugated 7-hydroxyflavone "C=O" stretching vibration band at 1624 cm^{-1}, the aromatic nucleus vibrational absorption bands at 1513 cm^{-1}, the antisymmetric stretching vibration of "C-H" and aryl ethers "=C-O-C" at 2932 cm^{-1} and 1265 cm^{-1}, and the out-of-plane bending of benzene ring hydrogen vibration absorption bands at 817 and 779 cm^{-1}. The presence of characteristic absorption band at 1075 cm^{-1} suggests that it may result from the stretching vibration of the glycosidic bond "C-O-C" or the in-plane bending vibration of the substituted benzene ring hydrogen.

Upon the formation of the flavonoids-APS complexes, the hydroxyl peak "-OH" undergoes a shifted from 3345 cm^{-1} to 3351 cm^{-1}. This shift suggests the occurrence of energy transfer through the formation of hydrogen bonds or π-π stacking interactions between the flavonoids and APS. Moreover, the blue shifts observed in the stretching vibration peak of "C-O-C" in the glycosidic bond and the appearance of new absorption peaks in the flavonoids-APS complexes indicate

the formation of weak bonding interactions between the flavonoids and APS. These weak bonds likely contribute to the stabilization of flavonoids-APS complexes. These findings are consistent with previous research outcomes. For instance, polysaccharide, as hydrophilic polymers, have been reported to self-assemble into nanoparticles through various non-covalent interactions, such as hydrophobic interaction, electrostatic adsorption, LJ, π-π bonding or other.[54,55]

Conclusion

This study aimed to investigate the impact of APS on the biopharmaceutical properties of four representative flavonoids both in vitro and in vivo. The results demonstrate that APS has the ability to self-assemble into nanoparticles, making it a promising carrier for enhancing the water solubility and stability of insoluble flavonoids in vitro. Furthermore, APS was found to increase the C_{max} and AUC_{0-t} of flavonoids in vivo. The study also examined the interaction mechanisms between APS and flavonoids using multispectral techniques and molecular dynamics simulations. It was revealed that APS can form weak intermolecular bonds, such as hydrogen bonds, with flavonoids, facilitating their self-assembly.

Notably, this study indicates the potential of APS to enhance the bioavailability of flavonoids, which is crucial for utilizing APS as a natural carrier to construct multi-component nano-co-delivery system. Self-assembly is a green method, is employed in this study, and natural polysaccharides possess favorable characteristics such as excellent biocompatibility, low toxicity, and low immunogenicity. The self-assembly of natural polysaccharides offers an eco-friendly approach that reduces the likelihood of harmful toxic cross-linking in biomedical applications.

In comparison to introducing external excipients, the use of natural polysaccharides derived from plants as carriers provides a unique advantage in enhancing dissolution, permeation and absorption. The discovery of the self-assembly properties of natural polysaccharides and their potential as carriers holds significant promise in the field of medical nanocarriers. These findings are particularly important in enhancing the stability and bioavailability of active components derived from natural plants.

Data Sharing Statement

The data that support the findings of this study are available from the corresponding author (Feng Liang) upon reasonable request.

Acknowledgments

This work was supported by the National Natural Science Foundation of China (No. 82204626, No. 82230117 and No. 81973536) and Jiangsu Funding Program for Excellent Postdoctoral Talent (No. 2022ZB317). We are grateful to the National Supercomputing Center in Wuxi for doing the numerical calculations in this study on its supercomputer system.

Author Contributions

All authors made a significant contribution to the work reported, whether that is in the conception, study design, execution, acquisition of data, analysis and interpretation, or in all these areas: took part in drafting, revising or critically reviewing the article; gave final approval of the version to be published; have agreed on the journal to which the article has been submitted; and agree to be accountable for all aspects of the work.

Disclosure

The authors report no conflicts of interest in this work.

References

1. Algahtani MS, Ahmad MZ, Nourein IH, et al. Co-Delivery of Imiquimod and Curcumin by Nanoemugel for Improved Topical Delivery and Reduced Psoriasis-Like Skin Lesions. *Biomolecules*. 2020;10(7):968. doi:10.3390/biom10070968
2. Jahangirian H, Ghasemian Lemraski E, Webster TJ, et al. A review of drug delivery systems based on nanotechnology and green chemistry: green nanomedicine. *Int J Nanomedicine*. 2017;12:2957–2978. doi:10.1016/j.msec.2021.112039
3. Li M, Sun X, Yin M, et al. Recent Advances in Nanoparticle-Mediated Co-Delivery System: a Promising Strategy in Medical and Agricultural Field. *Int J Mol Sci*. 2023;24(6). doi:10.3390/ijms24065121

4. Lin X, Huang X, Tian X, et al. Natural Small-Molecule-Based Carrier-Free Self-Assembly Library Originated from Traditional Chinese Herbal Medicine. *Acs Omega*. 2022;7(48):43510–43521. doi:10.1021/acsomega.2c04098
5. Huang J, Zhu Y, Xiao H, et al. Formation of a traditional Chinese medicine self-assembly nanostrategy and its application in cancer: a promising treatment. *Chin Med*. 2023;18(1):66. doi:10.1186/s13020-023-00764-2
6. Xiong J, Jiang B, Luo Y, et al. Multifunctional Nanoparticles Encapsulating Astragalus Polysaccharide and Gold Nanorods in Combination with Focused Ultrasound for the Treatment of Breast Cancer. *Int J Nanomedicine*. 2020;15:4151–4169. doi:10.2147/ijn.S246447
7. Wu D-T, He Y, Fu M-X, et al. Structural characteristics and biological activities of a pectic-polysaccharide from okra affected by ultrasound assisted metal-free Fenton reaction. *Food Hydrocoll*. 2022;122:107085. doi:10.1016/j.foodhyd.2021.107085
8. Mizrahy S, Peer D. Polysaccharides as building blocks for nanotherapeutics. *Chem Soc Rev*. 2012;41(7):2623–2640. doi:10.1039/c1cs15239d
9. Samrot AV, Kudaiyappan T, Bisyarah U, et al. Extraction, Purification, and Characterization of Polysaccharides of Araucaria heterophylla L and Prosopis chilensis L and Utilization of Polysaccharides in Nanocarrier Synthesis. *Int J Nanomedicine*. 2020;15:7097–7115. doi:10.2147/IJN.S259653
10. Liu F, Sun L, You G, et al. Effects of Astragalus polysaccharide on the solubility and stability of 15 flavonoids. *Int J Biol Macromol*. 2020;143:873–880. doi:10.1016/j.ijbiomac.2019.09.148
11. Xavier M, Garcia-Hevia L, Amado IR, et al. In Vitro Intestinal Uptake And Permeability Of Fluorescently-Labelled Hyaluronic Acid Nanogels. *Int J Nanomedicine*. 2019;14:9077–9088. doi:10.2147/IJN.S224255
12. Sun L, You G, Zheng F, et al. In vitro and in vivo evaluation of the influences of polysaccharides derived from Glycyrrhiza uralensis on three alkaloids and potential interaction mechanisms. *Int J Biol Macromol*. 2020;157:452–460. doi:10.1016/j.ijbiomac.2020.04.140
13. Fu Z, Han L, Zhang P, et al. Cistanche polysaccharides enhance echinacoside absorption in vivo and affect the gut microbiota. *Int J Biol Macromol*. 2020;149:732–740. doi:10.1016/j.ijbiomac.2020.01.216
14. Wang B, Huang B, Yang B, et al. Structural elucidation of a novel polysaccharide from Ophiopogonis Radix and its self-assembly mechanism in aqueous solution. *Food Chem*. 2023;402:134165. doi:10.1016/j.foodchem.2022.134165
15. Yang B, Yang N, Chen Y, et al. An Integrated Strategy for Effective-Component Discovery of Astragali Radix in the Treatment of Lung Cancer. *Front Pharmacol*. 2021;11:580978. doi:10.3389/fphar.2020.580978
16. Su H-F, Shaker S, Kuang Y, et al. Phytochemistry and cardiovascular protective effects of Huang-Qi (Astragali Radix). *Med Res Rev*. 2021;41(4):1999–2038. doi:10.1002/med.21785
17. Du Y, Li C, Xu S, et al. LC-MS/MS combined with blood-brain dual channel microdialysis for simultaneous determination of active components of astragali radix-safflower combination and neurotransmitters in rats with cerebral ischemia reperfusion injury: application in pharmacokinetic and pharmacodynamic study. *Phytomedicine*. 2022;106:154432. doi:10.1016/j.phymed.2022.154432
18. Yang B, Xiong Z, Lin M, et al. Astragalus polysaccharides alleviate type 1 diabetes via modulating gut microbiota in mice. *Int J Biol Macromol*. 2023;234:123767. doi:10.1016/j.ijbiomac.2023.123767
19. Malde AK, Zuo L, Breeze M, et al. An Automated Force Field Topology Builder (ATB) and Repository: version 1.0. *J Chem Theory Comput*. 2011;7(12):4026–4037. doi:10.1021/ct200196m
20. Stroet M, Caron B, Visscher KM, et al. Automated Topology Builder Version 3.0: prediction of Solvation Free Enthalpies in Water and Hexane. *J Chem Theory Comput*. 2018;14(11):5834–5845. doi:10.1021/acs.jctc.8b00768
21. Wu J, Li C, Bai L, et al. Structural differences of polysaccharides from Astragalus before and after honey processing and their effects on colitis mice. *Int J Biol Macromol*. 2021;182:815–824. doi:10.1016/j.ijbiomac.2021.04.055
22. Zhang J, Lu T. Efficient evaluation of electrostatic potential with computerized optimized code. *Phys Chem Chem Phys*. 2021;23(36):20323–20328. doi:10.1039/d1cp02805g
23. Lu T, Chen F. Multiwfn: a multifunctional wavefunction analyzer. *J Comput Chem*. 2012;33(5):580–592. doi:10.1002/jcc.22885
24. Piazzini V, Rosseti C, Bigagli E, et al. Prediction of Permeation and Cellular Transport of Silybum marianum Extract Formulated in a Nanoemulsion by Using PAMPA and Caco-2 Cell Models. *Planta Med*. 2017;83(14–15):1184–1193. doi:10.1055/s-0043-110052
25. Yang H, Zhai B, Wang M, et al. The influence of rhein on the absorption of rehmaionoside D: in vivo, in situ, in vitro, and in silico studies. *J Ethnopharmacol*. 2022;282:114650. doi:10.1016/j.jep.2021.114650
26. Pan Y, Qian D, Liu P, et al. The influence of essential oils from Xiang-Fu-Si-Wu Decoction on its non-volatile components and its application for pharmacokinetics in normal rats. *J Chromatogr B*. 2017;1060:221–230. doi:10.1016/j.jchromb.2017.06.004
27. Li T, Wang P, Guo W, et al. Natural Berberine-Based Chinese Herb Medicine Assembled Nanostructures with Modified Antibacterial Application. *ACS Nano*. 2019;13(6):6770–6781. doi:10.1021/acsnano.9b01346
28. Zhang H, Zhu Y, Sun C, et al. GSH responsive nanomedicines self-assembled from small molecule prodrug alleviate the toxicity of cardiac glycosides as potent cancer drugs. *Int J Pharmaceut*. 2020;575:118980. doi:10.1016/j.ijpharm.2019.118980
29. Zhuang Y, Yan J, Zhu W, et al. Can the aggregation be a new approach for understanding the mechanism of Traditional Chinese Medicine? *J. Ethnopharmacol*. 2008;117(2):378–384. doi:10.1016/j.jep.2008.02.017
30. Li N, Zhou T, Wu F, et al. Pharmacokinetic mechanisms underlying the detoxification effect of Glycyrrhizae Radix et Rhizoma (Gancao): drug metabolizing enzymes, transporters, and beyond. *Expert Opin Drug Met*. 2019;15(2):167–177. doi:10.1080/17425255.2019.1563595
31. Takagi T, Ramachandran C, Bermejo M, et al. A provisional biopharmaceutical classification of the top 200 oral drug products in the United States, Great Britain, Spain, and Japan. *Mol Pharm*. 2006;3:631–643. doi:10.1021/mp0600182
32. Kalepu S, Nekkanti V. Insoluble drug delivery strategies: review of recent advances and business prospects. *Acta Pharm Sin B*. 2015;5(5):442–453. doi:10.1016/j.apsb.2015.07.003
33. Munir MU, Ikraam M, Nadeem M, et al. Fabrication, In Vitro and In Vivo Evaluation of Non-Ordered Mesoporous Silica-Based Ternary Solid Dispersions for Enhanced Solubility of Flurbiprofen. *Pharmaceuticals*. 2022;15(7):856. doi:10.3390/ph15070856
34. Vincent K, Cornea VM, Jong YI, et al. Intracellular mGluR5 plays a critical role in neuropathic pain. *Nat Commun*. 2016;7:10604. doi:10.1038/ncomms10604
35. Olivas-Aguirre FJ, Mendoza S, Alvarez-Parrilla E, et al. First-Pass Metabolism of Polyphenols from Selected Berries: a High-Throughput Bioanalytical Approach. *Antioxidants*. 2020;9(4):311. doi:10.3390/antiox9040311
36. González-Berdullas P, Pereira RB, Teixeira C, et al. Discovery of the Anticancer Activity for Lung and Gastric Cancer of a Brominated Coelenteramine Analog. *Int J Mol Sci*. 2022;23(15):8271. doi:10.3390/ijms23158271

37. Granata G, Paterniti I, Geraci C, et al. Potential Eye Drop Based on a Calix[4]arene Nanoassembly for Curcumin Delivery: enhanced Drug Solubility, Stability, and Anti-Inflammatory Effect. *Mol Pharmaceut*. 2017;14(5):1610–1622. doi:10.1021/acs.molpharmaceut.6b01066
38. Li F, Liu B, Li T, et al. Review of Constituents and Biological Activities of Triterpene Saponins from Glycyrrhizae Radix et Rhizoma and Its Solubilization Characteristics. *Molecules*. 2020;25(17). doi:10.3390/molecules25173904
39. Parekh PY, Patel VI, Khimani MR, et al. Self-assembly of bile salts and their mixed aggregates as building blocks for smart aggregates. *Adv Colloid Interfac*. 2023;312:102846. doi:10.1016/j.cis.2023.102846
40. Stoffelen C, Huskens J. Soft Supramolecular Nanoparticles by Noncovalent and Host–Guest Interactions. *Small*. 2016;12(1):96–119. doi:10.1002/smll.201501348
41. Fan Y, Liu Y, Wu Y, et al. Natural polysaccharides based self-assembled nanoparticles for biomedical applications – a review. *Int J Biol Macromol*. 2021;192:1240–1255. doi:10.1016/j.ijbiomac.2021.10.074
42. Khare T, Palakurthi SS, Shah BM, et al. Natural Product-Based Nanomedicine in Treatment of Inflammatory Bowel Disease. *Int J Mol Sci*. 2020;21(11). doi:10.3390/ijms21113956
43. Kotla NG, Rana S, Sivaraman G, et al. Bioresponsive drug delivery systems in intestinal inflammation: state-of-The-art and future perspectives. *Adv Drug Deliver Rev*. 2019;146:248–266. doi:10.1016/j.addr.2018.06.021
44. Zhao G, Hong L, Liu M, et al. Isolation and Characterization of Natural Nanoparticles in Naoluo Xintong Decoction and Their Brain Protection Research. *Molecules*. 2022;27(5). doi:10.3390/molecules27051511
45. Musa N, Wong TW. Design of polysaccharidic nano-in-micro soft agglomerates as primary oral drug delivery vehicle for colon-specific targeting. *Carbohyd Polym*. 2020;247:116673. doi:10.1016/j.carbpol.2020.116673
46. Zhou P, Feng R, Luo Z, et al. Synthesis, identification and bioavailability of Juglans regia L. polyphenols-Hohenbuehelia serotina polysaccharides nanoparticles. *Food Chem*. 2020;329:127158. doi:10.1016/j.foodchem.2020.12715
47. Hu B, Han L, Ma R, et al. All-Natural Food-Grade Hydrophilic–Hydrophobic Core–Shell Microparticles: facile Fabrication Based on Gel-Network-Restricted Antisolvent Method. *ACS Appl Mater Inter*. 2019;11(12):11936–11946. doi:10.1021/acsami.9b00980
48. Han X, Lu Y, Xie J, et al. Zwitterionic micelles efficiently deliver oral insulin without opening tight junctions. *Nat Nanotechnol*. 2020;15(7):605–614. doi:10.1038/s41565-020-0693-6
49. Wang Z-H, Chu M, Yin N, et al. Biological chemotaxis-guided self-thermophoretic nanoplatform augments colorectal cancer therapy through autonomous mucus penetration. *Sci Adv*. 2022;8(26):3917. doi:10.1126/sciadv.abn3917
50. Liu J, Wang X, Yong H, Kan J, Jin C. Recent advances in flavonoid-grafted polysaccharides: synthesis, structural characterization, bioactivities and potential applications. *Int J Biol Macromol*. 2018;116:1011–1025. doi:10.1016/j.ijbiomac.2018.05.149
51. Khan S, Hussain A, Attar F, et al. A review of the berberine natural polysaccharide nanostructures as potential anticancer and antibacterial agents. *Biomed Pharmacother*. 2022;146:112531. doi:10.1016/j.biopha.2021.112531
52. Wen L, Jiang Y, Yang J, et al. Structure, bioactivity, and synthesis of methylated flavonoids. *Ann N Y Acad Sci*. 2017;1398(1):120–129. doi:10.1111/nyas.13350
53. Takahama U, Hirota S. Interactions of flavonoids with alpha-amylase and starch slowing down its digestion. *Food Funct*. 2018;9(2):677–687. doi:10.1039/C7FO01539A
54. Bianchera A, Bettini R. Polysaccharide nanoparticles for oral controlled drug delivery: the role of drug–polymer and interpolymer interactions. *Expert Opin Drug Del*. 2020;17(10):1345–1359. doi:10.1080/17425247.2020.1789585
55. Rehman A, Jafari SM, Tong Q, et al. Drug nanodelivery systems based on natural polysaccharides against different diseases. *Adv Colloid Interfac*. 2020;284:102251. doi:10.1016/j.cis.2020.102251